small NANO MICRO

Virtual Micropores

Tunable Aqueous Virtual Micropore

*Jae Hyun Park, Weihua Guan, Mark A. Reed, and Predrag S. Krstić**

***A** charged microparticle can be trapped in an aqueous environment by forming a narrow virtual pore—a cylindrical space region in which the particle motion in the radial direction is limited by forces emerging from dynamical interactions of the particle charge and dipole moment with an external radiofrequency quadrupole electric field. If the particle satisfies the trap stability criteria, its mean motion is reduced exponentially with time due to the viscosity of the aqueous environment; thereafter the long-time motion of particle is subject only to random, Brownian fluctuations, whose magnitude, influenced by the electrophoretic and dielectrophoretic effects and added to the particle size, determines the radius of the virtual pore, which is demonstrated by comparison of computer simulations and experiment. The measured size of the virtual nanopore could be utilized to estimate the charge of a trapped micro-object.*

1. Introduction

The trapping, localization, and manipulation of biomolecules which are typically stable only in an aqueous environment are of critical importance to various biotechnical and medical applications. A 2D aqueous quadrupole trap (AQT) forms a cylindrical confining region for a charged particle in the trap stability region, an "aqueous virtual pore" (AVP), offers a possibility for such applications. The quadrupole trap, based on the combination of static (DC) and radiofrequency (rf, AC) electric fields and developed for vacuum applications is also known as Paul trap.[1,2] We have demonstrated, both theoretically and experimentally, that the similar trapping principle can be utilized in the water environment.[3,4] Similarly, Kloepper et al.[5] examined the slow-down of mobility of highly conductive charged Au particles in water under AC electrophoresis in simple geometry. While the secular and micro motions of the stable charged particle in an AQT diminishes exponentially with time due to the water viscosity, the radius of the AVP is determined by the rms (root-mean-squared) value of the thermal random fluctuations of the particle motion in water, added to the particle radius, as shown in **Figure 1**. A robust, stable trapping is possible with a quadrupole AC field only, aided in AQT by the high viscosity of water.[3,4] The purpose of this study is the extension and precious quantification of AVP in previous studies.[4]

The dynamical features of the particle-water trap system in the presence of only AC electrophoretic (EP) forces are characterized by two dimensionless parameters, q and b. The q-parameter represents the characteristic magnitude of EP force from the AC field, $q = 2QU/Mr_0^2\Omega^2$, where M and Q are the mass and charge of the particle, U and Ω are the amplitude and angular frequency of the applied quadrupole field, and r_0 is the trap size (see Figure 1). The b-parameter, $b = 2\xi/M\Omega$, characterizes the medium viscosity, where ξ is the friction coefficient of a non-slip spherical particle in Stokes' drag. The stability and motion of the particle in AQT could also be affected by dielectrophoretic (DEP) forces, emerging from vastly different relative dielectric constants of water (~80) and the microparticle (~3), which is in our experiment a polystyrene bead of average radius of 490 nm, and density of 1050 kg/m^3. The surface of the beads is functionalized with COOH groups, causing a negative charging

Dr. J. H. Park, Dr. P. S. Krstić
Physics Division
Oak Ridge National Laboratory
PO Box 2008, Bldg. 6010, Oak Ridge, TN 37831, USA
E-mail: krsticp@ornl.gov
Phone: +1-865-574-4701; Fax: +1-865-574-1118
W. Guan, Prof. M. A. Reed
Department of Electrical Engineering
Yale University
New Haven, CT 06520, USA
Prof. M. A. Reed
Department of Applied Physics
Yale University
New Haven, CT 06520, USA

DOI: 10.1002/smll.201101739

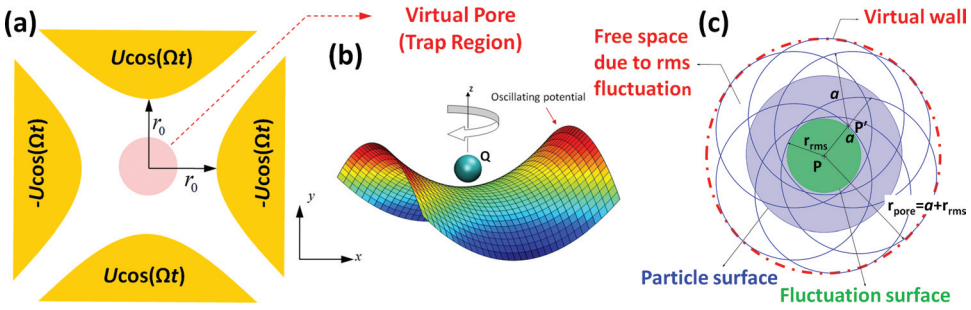

Figure 1. a) Schematic diagram of 2D AQ trap with pure AC electric field. Under the stable conditions, a virtual pore (pink region) is formed around the trap axis, with the ability to confine particles. The pore is not limited in the z-direction. b) In the AVP, a particle performs the random motion around the saddle point of oscillating potential. c) The pore radius, r_{pore}, is determined by the amplitude of the random motion and the particle size. A spherical particle surface, centered at P, is depicted by a filled blue circle (of radius *a*). Hollow blue circles represent the displacement of the particle by random fluctuations. The green circle (radius of r_{rms}) indicates the region of the fluctuations of the particle center-of-mass (fluctuation surface). The red dashed dot circle is the radius of AVP given as $r_{pore} = a + r_{rms}$ (virtual wall). Note that the virtual wall and fluctuation surface are the mean values, with uncertainties defined by the width of the distributions of r_{rms} values, as shown in Figure 2b and Figure 3b.

when embedded in water.[4] Interestingly, when the stability is concurrently controlled by both DEP and EP forces, the DEP forces are influential only for q << 1 (see Supporting Information, SI1).

The main advantage of an AVP using AQT over physical nanopores such as solid-state nanopores,[6] α-hemolysin,[7] and carbon nanotubes[8] is relaxation of critical dimension control, which simplifies the device fabrication. The radial dimension of desired trapping could be significantly smaller than the actual fabricated dimensions. Moreover, the translocation of biomolecules (e.g., DNA, RNA, protein, etc.) through the AVP is free from any influence of the pore surface and therefore the motion can be more easily controlled. On the other hand, the AQT can also have some advantages over the optical traps which are used to manipulate biomolecules. One of the drawbacks of optical traps is the high energy density at the focus of the trap, causing heating-induced damages of the trapped material.[9] The power density in the AVP of the AQT is many orders of magnitude smaller than in the optical traps.

2. Results and Discussion

A remarkable property of an AVP is that its radial size can be tuned with only two input variables, AC voltage and frequency, which control the rms fluctuations of the particle. We theoretically analyze the long-time rms fluctuations of the spherical charged polystyrene bead in a linear (two-dimensional) micro-AQT which we experimentally validate by the planar aqueous micro trap, shown to successfully reproduce two-dimensional trapping dynamics.[4] The geometry and the AC potential of the AQT is illustrated in Figure 1, and the corresponding Langevin-type equation of motion (EOM) of the charged particle in the trap has the form (For the two-dimensional EOM, please refer to Supporting Information SI2)

$$\frac{d^2x}{d\tau^2} = -b\frac{dx}{d\tau} + 2q\cos(2\tau)\,x + r_m\left[\mathrm{Re}(fCM) + \mathrm{Re}(fCM)\cos(4\tau) - \mathrm{Im}(fCM)\sin 4\tau\right]x + \frac{2}{\Omega}R\left(\frac{2\tau}{\Omega}\right) \quad (1)$$

where τ is the dimensionless time and x = (MΩ/2)X is a transformed variable of physical coordinate X, b and q are dimensionless parameters defined above, f_{CM} is the Clausius-Mossoti factor (see Supporting Information SI3), and R is the "white" random force (see Supporting Information SI2).[10] Compared to a conventional Paul trap in vacuum or in a buffer gas, the motion of charged particles in an AQT is controlled by both EP and DEP. The terms on the right-hand-side of Equation (1) are the damping force, EP force due to the AC potential, DEP force due to the polarizability difference between the medium and the particle, and the Brownian random force, respectively. The characteristic magnitude of the DEP force is defined by $r_m = 8\pi a^3 \varepsilon_m \varepsilon_0 U^2 / M r_0^4 \Omega^2$ where *a* is particle size, ε is relative dielectric constant and ε_0 is the vacuum permittivity ($\varepsilon_0 = 8.85 \times 10^{-12}$ F/m). The period-averaged rms fluctuations of a particle coordinate in the long-time limit are computed from Equation (1) using Green function techniques and a random phase approach (see Experimental Section). Ideally, the rms fluctuations are the same in both x and y directions. Since the z-dimension is sufficiently long (ideally infinite), fluctuations in the z-direction are not of interest in this study.

For experimental verification, we fabricated a planar AQ microtrap, which simulates well a linear trap,[4] with size of r_0 = 4 μm and trapped a single charged polystyrene bead in de-ionized (DI) water at room temperature (T = 300 K) (see Experimental Section). The conductivity of DI water is as small as 5.5 μS/m, therefore its effect is negligible. The trapping study in electrolyte is under way. Trapping mostly occurs for a single particle (instead of ensembles), most probably due to interparticle Coulomb repulsion. The videos for particle trapping experiments are available online as Supporting Information to the provided reference.[4] The AC voltage, U, and the frequency, f = Ω/2π, were varied from 0.92 V to 1.82 V and from 1.3 MHz to 3.0 MHz, respectively. These voltage and frequency ranges are determined by the parameters of the trapped particle, and the physical trap design (which can be scaled if desired). These resulted in b-values of the order of unity and in q-values of the order of 10^{-3}. For this small q << 1, mainly caused by the microsize of trap and smallness

NANO MICRO small

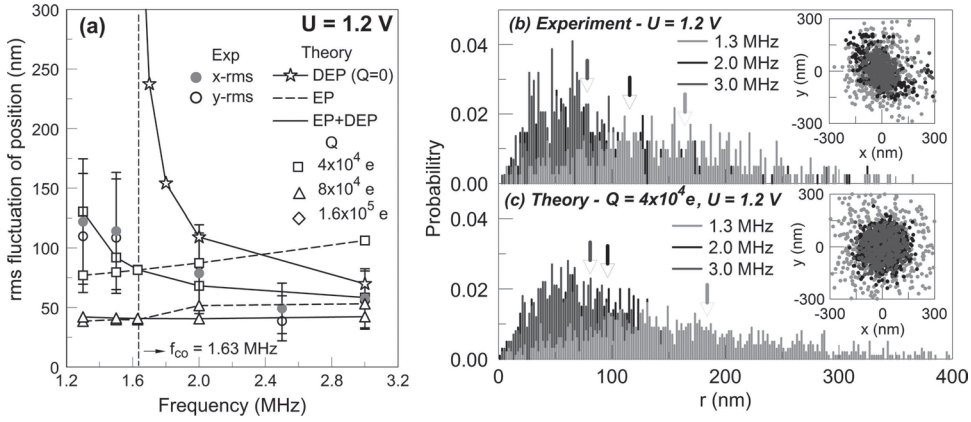

Figure 2. a) Variation of x-directional mean rms fluctuations of the particle center with driving frequency when AC voltage is fixed at 1.2 V. The filled red and blue hollow circles are the measured mean rms fluctuations of x-coordinate and y-coordinate, respectively, with 40% error margin. The cross-over frequency, f_{co}, is 1.63 MHz (Figure S2). b,c) Scatter plots of the particle (insets) and the corresponding radial distributions for various AC frequencies of 1.3 (light grey), 2.0 (black), and 3.0 (dark grey) MHz at AC voltage fixed at 1.2 V. Each point indicates the fluctuations of the center-of-mass of particle: b) experimental data; c) theoretical prediction with $Q = 4.0 \times 10^4$ *e*. The circular areas in scatter plots correspond to the fluctuation surfaces in Figure 1 (filled green circle). The arrows indicate the mean radial distributions at the corresponding frequencies, the widths of the distributions are discussed in the Supporting Information SI5.

of the Q/M for the polystyrene bead, the stability of the particle is influenced by both EP and DEP (Figure S1).

In **Figure 2**a, the computed (period averaged) rms fluctuations of center of mass of particle for DEP-only (zero charge (Q = 0), q = 0 in Equation (1)), EP-only ($r_m = 0$), and EP + DEP (simultaneous consideration of EP and DEP, $q \neq 0$ and $r_m \neq 0$) are compared with the measurements for various frequencies at a fixed voltage of 1.20 V. The frequency is scanned from the unstable positive DEP region (pDEP, f = 1.3 MHz < f_{co}) to the stable negative DEP region (nDEP, f = 3.0 MHz > f_{co}) (see Supporting Information SI3). For EP and EP + DEP simulations, two fixed particle charges of $Q = 4.0 \times 10^4$ *e* and 8.0×10^4 *e* are considered (*e* is the unit charge, $e = 1.6 \times 10^{-19}$ C). It is obvious from the Figure 2a that the qualitative trends of DEP, EP, and EP+DEP curves are quite different. The DEP fluctuations diverge (becoming larger than the trap size, r_0 = 4 μm) as the frequency approaches the cross-over (even from the nDEP regime), implying that DEP has a simple stability diagram with a single border, f_{co}, separating unstable region for $f < f_{co}$ and stable for $f > f_{co}$. Contrary to the DEP-controlled random fluctuations of the particle, the EP-controlled fluctuations increase with frequency (i.e., with a decrease of the q-parameter) (see Supporting Information SI4). The combination of EP and DEP provides a successful prediction of the experimental observations, i.e., that the rms fluctuations 1) are finite in the pDEP region; and 2) decreasing with increasing frequency. The remarkable quantitative agreement of theoretical predictions and experimental data is established only by common action of DEP and EP with $Q = 4.0 \times 10^4$ *e*. The EP + DEP simulations with larger charge, $Q = 8.0 \times 10^4$ *e*, does not reproduce the experimental trend, resulting in the curve with local minimum at the cross-over frequency, which increases with $f > f_{co}$. The significant influence of DEP is unexpected considering that the magnitude ratio of DEP to EP force is small here ($\frac{r_m}{q} = \frac{4\pi a^3 \varepsilon_m \varepsilon_0 U}{r_0^2 Q} = 1.20 \times 10^{-2}$, even though $q << 1$ ($q = 2.78 \times 10^{-3}$ for f = 1.3 MHz to $q = 1.45 \times 10^{-3}$ for f = 1.8 MHz). The b-parameter is of the order of one. Neither DEP-only nor EP-only reproduces the experimental trend. The computations with a proper fixed charge successfully predict the experimental observations, implying that the polystyrene bead charge is not a function of the AC-field frequency.

Based on the discussion above, we can state that the *formation of stable virtual pore in an aqueous quadrupole trap is possible even in the pDEP regime*. The comparisons of the scatter plot (insets in Figure 2b,c) and the corresponding radial position distributions in Figure 2b,c confirm this conclusion but also stress the significance of simultaneous action of EP and DEP in a virtual pore for a correct understanding of an AQ microtrap. The scatter plot presents the fluctuations of the particle center of mass and the circular confinement region forms the fluctuation surface. The radius of the scatter plot R_{sc} (for example, green points in Figure 2c) is determined not only by the mean rms fluctuations (arrows in Figure 2b for the r-fluctiations), but also by the widths of the distribution. Thus in Figure 2c the r_{rms} of Figure 1c is 82.89 nm for f = 3.0 MHz, while its width, defined as one standard deviation, is σ_{rms} = 38.64 nm, defining the uncertainty of the virtual pore radius, r_{pore}, in Figure 1c. We note that the fluctuations in the radial coordinate r, defined as $\sqrt{\langle r^2 \rangle} = \sqrt{\langle x^2 + y^2 \rangle}$, are larger than $\sqrt{\langle x^2 \rangle}$ and $\sqrt{\langle y^2 \rangle}$ by $\sqrt{2}$ in average. This is further discussed in the Supporting Information SI5.

Figure 3a shows the variation of the mean rms fluctuations of center of mass of a charged particle in the AQT with AC voltage for a fixed driving frequency $f = \Omega/2\pi = 3.0$ MHz. This frequency belongs to the strong nDEP regime, in which the time-average DEP force acts toward the trap center. For EP and EP+DEP cases, three different values for the bead charge, $Q = 4.0 \times 10^4$ *e*, 8.0×10^4 *e*, and 1.6×10^5 *e* were considered and compared with the experimental data (the bead, used for the measurement, is different than the one of Figure 2). The variations of AC voltage and the particle charge cause

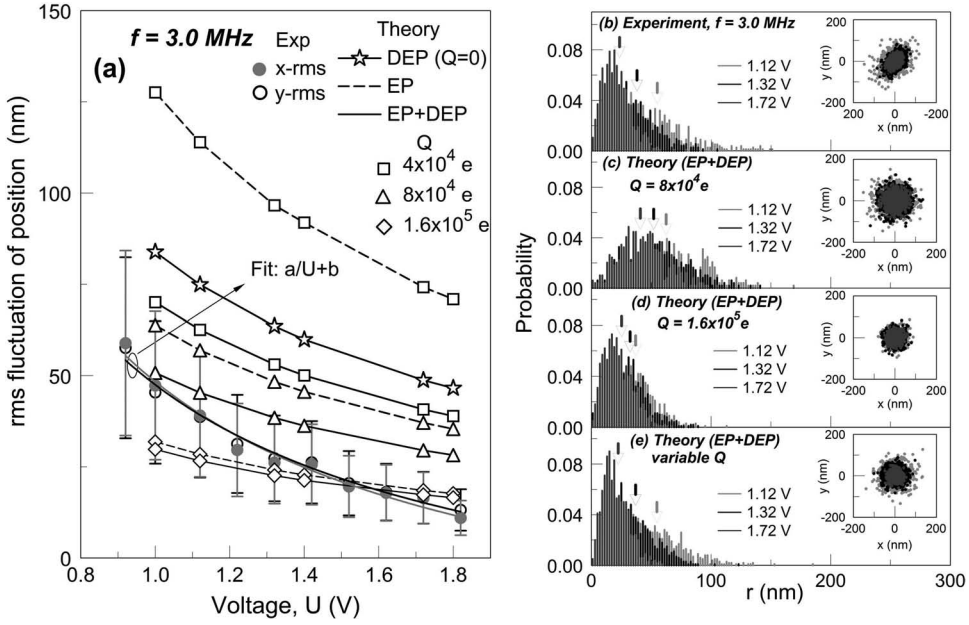

Figure 3. a) Variations of x-rms fluctuations of the center of mass of spherical charged particle with AC voltage for a fixed frequency and for three different charges of Q = 4.0×10^4 *e*, 8.0×10^4 *e*, and 1.6×10^5 *e*. The driving frequency is f = $\Omega/2\pi$ = 3 MHz. The experimental data x- and y- directions are almost coinciding, and have 40% error margin. The experimental data can be fitted well with a/U+b. For x-rms fluctuations, a = 82.28 and b = –33.92 and for y-fluctuations, a = 77.27 and b = –29.75. b–e) Scatter plots of particle (insets) and the corresponding radial distributions for various AC voltages of 1.12 V (light grey), 1.32 V (black), and 1.72 V (dark grey): b) experimental data; c) simulation results with Q = 8.0×10^4 *e* (EP + DEP); d) Q = 1.6×10^5 *e* (EP + DEP); and e) variable Q's, Q/10^5 *e* = cU + d, with c = 1.44 [V^{-1}] and d = -0.65 (EP + DEP). The circular areas formed by the particle center-of-mass in the scatter plots correspond to the fluctuation surfaces in Figure 1. The arrows indicate the means of radial distributions at the corresponding voltage.

the change of the trap q-parameter, while b stays constant at 1.69. Thus, q = 3.10×10^{-2} for U = 1.8 V and Q = 1.6×10^5 *e*, while q = 4.35×10^{-3} for U = 1.0 V and Q = 4.0×10^4 *e*. For both DEP-only and EP-only cases, the mean rms fluctuations always decrease with increase of V since both restoring forces, EP and DEP, increase with voltage ($r_m \propto U^2$ and $q \propto U$). A larger restoring force suppresses the fluctuations (e.g., the harmonic external excitation[11] and EP-only microtrap[12]).

The DEP curve in Figure 3a shows significantly larger mean rms fluctuations from the experimentally observed ones. With addition of EP, the EP + DEP curve (Q = 4.0×10^4 *e*, 8.0×10^4 *e*, and Q = 1.6×10^5 *e*) shifts toward the experimental data. The curve with Q = 8.0×10^4 *e* shows a good match with experiment in the low voltage region, but overestimates fluctuations in higher voltage region while the EP + DEP curve with higher charge of Q = 1.6×10^5 *e* shows a good agreement in the high voltage region, but underestimates experiments in the low voltage region. This discrepancy suggests that Q might vary with U. Remarkably, a linear fitting relation, $\frac{Q}{10^5 e} = cU + d$ with c = 1.44 [V^{-1}] and d = –0.65, produces an excellent agreement with experiment (Figure S5c). This indicates that the effective charge of the bead might increase with the applied voltage, relying on the complicated electrochemical processes including dissociation of chemical group on particle surface (e.g., COOH on polystyrene bead[4]).

The comparison of EP + DEP and EP-only results yields two interesting observations: (1) The simultaneous consideration of DEP and EP suppresses the fluctuations and the resultant rms fluctuations are always smaller than those in DEP-only cases; (2) The upper and lower limits of the AVP size are determined by the rms fluctuations due to DEP and EP, respectively. The larger difference between EP and EP + DEP curve is observed for the smaller charge. The reason for observation (1) is simple: The present DEP is in the nDEP regime, it adds its restoring effects to those of the EP. The second observation is interesting because the amplitude of the DEP force (~$r_m = 1.42 \times 10^{-4}$) is only 2% of EP force (q = 7.83×10^{-3}). This is consistent with Figure 2a, where we showed a significant role of small DEP force. The points (1) and (2) indicate that for small q << 1 the precise quantitative estimation of rms fluctuations in AQT requires simultaneous consideration of EP and DEP.

The sensitivity of fluctuations to the particle charge suggests a novel method for the estimation of the effective particle charge in an aqueous medium, which is essential in various biological diagnostics including protein analysis,[13] and is usually sensitive to the environmental conditions (e.g., pH).[14] The procedure assumes trapping of a charged particle using AQT and measuring the rms fluctuations. This results in an inverse problem of particle charge, Q, i.e., solving Equation (1) for various Q's using the experimental parameters, and finding Q which produces the best match with the measured fluctuations.

In Figure 3(b–d) we compare experimental data with the computed scatter plots (inset) and the radial distributions for two fixed charges, Q = 8.0×10^4 *e*, Q = 1.6×10^5 *e*, while varying U for a fixed frequency. In Figure 3e we vary the charges with U (Q = 7.98×10^4 *e* for 1.00 V, Q = 1.26×10^5 *e*

NANO MICRO small

for 1.32 V, Q = 1.84 × 10^5 *e* for 1.72 V) to fit the experimental data, obtained by varying U for fixed Ω. We take into account both EP and DEP in all computations. The scatter plots and radial distributions for the center of mass of particle confirm the findings from Figure 3a that the charge varies with U. The scatter plots also illustrate that the radial magnitude of rms fluctuation changes with voltage and charge, ranging from $r_{rms} \pm \sigma_{rms}$ = 62.59 ± 28.84 nm (for U = 1.12 V and Q = 8.0 × 10^4 *e*) to 22.44 ± 10.64 nm (for U = 1.8 V and Q = 1.6 × 10^5*e*). Mean rms fluctuations for various voltages are indicated with arrows in Figures 3 (b–e). The resulting radii of virtual pore are $a + r_{rms} \pm \sigma_{rms}$, where a = 490 nm in this case.

Based on successful comparison of the measured and simulated rms fluctuations and the virtual size trap for a microparticle in a micrometer trap, we extend our simulation by varying the particle size and charge, as well as the trap size and frequency of the applied voltage. In this we assume that the surface charge and volume mass density stay constant, defined by the spherical polystyrene bead in Figure 2. The mean rms fluctuations in r are reduced from 81.25 ± 38.98 nm to 10.80 ± 5.19 nm when the particle size is varied from $2a$ = 980 nm in a 8 μm-microtrap to $2a$ = 10 nm in a 81.63 nm nanotrap (U = 1.2 V, f = 3.0 MHz). As discussed in Reference [15] and the Supporting Information SI7, the stiffness of the trap in the presence of both EP and DEP forces in an AQT is $k_{eff} = k_{EP} + k_{DEP}$, resulting in the $1/k_{eff}$ scale (per unit force) for the rms fluctuations. This scale is dominated with a larger of k_{EP} and k_{DEP}, as seen from the Figure S6, showing that the DEP effect takes over the control of the rms fluctuations when the trap size decreases together with the particle size, taken here as $a = r_0/8$ (Figure S7a). This is also indicated in the Supporting Information SI7, where we showed that $k_{EP} \propto a$ and $k_{DEP} \propto 1/a$. On the other hand, for a 10 nm nanoparticle, the mean rms fluctuations increase with increase of trap size (Figure S7b) (both of k_{EP} and k_{DEP} vary as $1/r_0^4$). The rms fluctuations of a 10 nm particle are weakly sensitive to the variation of particle charge (Figure S7c), while the variation with frequency decreases with the particle (and trap) size (Figure S7d).

The temperature influences only the random motion of the trapped particle in water because the magnitude of the random force is proportional to T, $G_R = 2k_BT\xi$ where k_B is the Boltzmann constant (1.38×10^{-23} J/K) and ξ is the Stokes friction coefficient (see SI3 in the Supporting Information), whereas the particle stability due to the mean-motion is not affected by temperature.[16] As a result, the magnitude of rms fluctuation is gradually increasing with T ($\sqrt{\bar{\sigma}_{xx}^{\infty}} \propto T^{1/2}$).[12]

3. Conclusion

To conclude, we investigated the features of a virtual pore formed in an AQ microtrap for the conditions for which EP and DEP effects are concurrent. The size of an AVP is determined by the long-time mean rms fluctuations superimposed to the particle size, with contributions of both EP and DEP. The uncertainty of the AVP size is determined by the width of the rms fluctuation distributions. The AVP's are proven stable even in pDEP regime and their size can be tuned with AC voltage and frequency. We performed a detailed comparison of experimental data and theoretical analysis, achieving a remarkable agreement. The close relation between rms fluctuations of the particle and its charge suggests a novel method for accurate experimental estimation of effective charge of a single biomolecule or generally a particle in a liquid.

Finally, the further miniaturization of the trap device might bring the realization of a few-nm virtual pore, which greatly relaxes many difficulties in fabrication and application of a physical nanopore. These expectations are supported by our theoretical predictions, which indicate reduction of the mean rms fluctuations and therefore reduction of the size of a virtual pore with decreasing the trap and the charged particle size.

The present study opens a new door to the utilization of the charges in micromolecules and nanoparticles for trapping, which is differentiated from the most previous trapping studies using the dielectrophoretic forces only.[17–23] Currently, we are trying to trap the charged biomolecules (e.g., DNA, protein) using AQT by reducing the trap size in electrolyte environment for the third-generation DNA sequencing applications.[24,25]

4. Experimental Section

Experiment: The planar quadrupole trapping devices are fabricated on a SiO2/Si wafer. A double-layer liftoff process is used to form the quadrupole electrodes. The microfluidic chamber is formed by poly(dimethylsiloxane) (PDMS) using epoxy (SU-8) as a molding master. Oxygen plasma treatment was used to permanently bond the PDMS to the device surface and form an anti-evaporation microfluidic channel. An inlet and an outlet were punched through before assembling. Once the device was assembled, it could be repeatedly used for a long time. We use a particle tracking algorithm to extract the motion fluctuations, which has been described in detail elsewhere[26] The videos are taken by a high-sensitivity digital CCD camera (Olympus DP70) with the highest shutter speed as fast as 1/44000 s. Videos are decomposed into frame sequences using the software VirtualDub (http://www.virtualdub.org/). The particle tracking is then carried out in NIH ImageJ platform (http://rsb.info.nih.gov/ij/) with a particle tracking plug-in tool developed by G. Levy (https://weeman.inf.ethz.ch/ParticleTracker/). As for the position variance extraction experiments, we set the shutter speed as 1/80 s and used a 100× objective.

The particles used in the experiments are polystyrene beads (Polysciences, Warrington, PA) of two diameters (0.481 ± 0.004 μm and 0.982 ± 0.013 μm). These are red-dyed. However, the color cannot be seen in the experiments because of the small size. (Usually it requires the size of the bead larger than 6 micrometers to see the color). The surface of these particles is functionalized with carboxylate group (-COOH). These COOH surface groups are the origin of the negative charges (COO-). Scanning electron microscopy (SEM) revealed that all the particles had a pronounced spherical shape. The solution used in the experiment was prepared by the following steps: (1)The beads were diluted to a density of ~10^6 particle/mL by deionized (DI) water (milli-Q grade, resistivity 18 MΩ·cm), in order to eliminate the particle-particle interactions during the experiment; (2) In order to thoroughly remove the

residual ions from the stock solution, the beads prepared in step (1) were washed five times in DI water by centrifuging the beads in a 10 mL tube at 13500 G for 10 min, re-suspending in DI water each time.

The prepared solution in the 10 mL tube was extracted and then pumped into the microfluidic chamber. The conductivity of the fresh suspension solution in the 10 mL tube (exposed to air) is measured as 0.1 μS/cm (EC 215 Multi-range Conductivity Meter, Hanna Instruments) and this slowly goes up to maximum 2.0 μS/cm during the course of an experiment (due to the absorption of ambient gas). This measured conductivity variation sets the lower and upper bound for the solution inside the microfluidic chamber. In fact, since the microfluidic channels are not directly exposed to air, little change of the solution conductivity inside the trap chamber is expected. Device fabrication is identical to that of a prior publication,[4] where more detailed information about the process can be found (included in the Supporting Information).

Computation of rms Fluctuation: The period-average rms fluctuations were computed by applying the Green's function transformation along with the random phase approaches to Equation (1). This method has been first proposed by Arnold et al.[12] In the random phase approach, instead of the random force, an arbitrary selected phase, $\varphi\varepsilon[0, 2\pi)$, is added to the 2τ and 4τ in sine and cosine functions. The computational procedure in the present study is the same as in Ref. 11 except replacing the EP force term $2q\cos(2\tau)$, with EP + DEP term

$$2q\cos(2\tau)x + r_m\left[\mathrm{Re}\left(f_{CM}\right) + \mathrm{Re}\left(f_{CM}\right)\cos(4\tau) - \mathrm{Im}\left(f_{CM}\right)\sin(4\tau)\right]x$$

The upper limit of integration was extended until the integrals converge, which is normally several hundred thousand periods. In this study, without loss of generality the period-average was performed over five different phases uniformly distributed from 0 to 2π, rather than from the random choice of phases. Since the average over hundred phases and that over five phases were identical within 0.01 nm (0.1 Å), we used the average over five phases in order to reduce the computational time.

Construction of Theoretical Scatter Plot: We first calculated form Equation (1) the period-averaged rms fluctuation in x-direction ($=\sqrt{\bar{\sigma}_{xx}^{\infty}}$–the values in Figure 1b), for each (b,q) pair. The x-coordinates of particles were randomly generated from the Gaussian distribution with the zero mean and the standard deviation of $\sqrt{\bar{\sigma}_{xx}^{\infty}}$. $\sqrt{\bar{\sigma}_{xx}^{\infty}}$ is theoretically same as the rms fluctuation in y-direction ($=\sqrt{\bar{\sigma}_{yy}^{\infty}}$). The y-coordinates were generated also from the same random Gaussian distribution. 1000 particles were collected to construct a scatter plot and corresponding radial distribution.

Supporting Information

Supporting Information is available from the Wiley Online Library or from the author.

Acknowledgements

This research was supported by the US National Human Genome Research Institute of the National Institutes of Health under grant No 1R21HG004764-02. PSK acknowledges partial support of the US Department of Energy at ORNL managed by a UT-Battelle for the US DOE under contract No DEAC05-00OR22725. JHP acknowledges support through ORNL Postdoctoral Program, administered by ORISE. The computations were performed on Kraken (a Cray XT5) at the National Institute for Computational Sciences (http://www.nics.tennessee.edu/), supported by the National Science Foundation.

[1] W. Paul, H. Steinwedel, *Z. Naturforschung A* **1953**, *8*, 448.
[2] W. Paul, *Rev. Mod. Phys.* **1990**, *62*, 531.
[3] X. Zhao, P. S. Krstić, *Nanotechnology* **2008**, *19*, 195702.
[4] W. Guan, S. Joseph, J. H. Park, P. S. Krstić, M. A. Reed, *Proc. Natl Acad. Sci. USA* **2011**, *108*, 9326.
[5] K. D. Kloepper, T.-D. Onuta, D. Amarie, B. Dragena, *J. Phys. Chem. B* **2004**, *108*, 2547.
[6] W. Timp, U. Mirsaidov, D. Wang, J. Comer, A. Aksimentiev, G. Timp, *IEEE Trans. Nanotechnol.* **2010**, *9*, 281.
[7] J. Clarke, H.-C. Wu, L. Jayasinghe, A. Patel, S. Reid, H. Bayley, *Nature Nanotechnol.* **2009**, *4*, 265.
[8] H. Liu, J. He, J. Tang, H. Liu, P. Pang, D. Cao, P. Krstić, S. Joseph, S. Lindsay, C. Nuckolls, *Science* **2010**, *327*, 64.
[9] K. C. Neuman, A. Nagy, *Nat. Meth.* **2008**, *5*, 491.
[10] W. T. Coffey, Yu. P. Kalmykov, J. T. Waldron, *The Langevin equation: with applications to stochastic problems in physics, chemistry and electrical engineering*, 2nd ed., World Scientific Publishing Co., Singapore **2004**.
[11] S. Chandrasekhar, *Rev. Mod. Phys.* **1943**, *15*, 1.
[12] S. Arnold, L. M. Folan, A. Korn, *J. Appl. Phys.* **1993**, *74*, 4291.
[13] M.-S. Chun, I. Lee, *Colloids Surf. A* **2008**, *318*, 191.
[14] D. J. Winzor, *Anal. Biochem.* **2004**, *325*, 1.
[15] W. Guan, J. H. Park, P. S. Krstić, M. A. Reed, *Nanotechnology* **2011**, *22*, 245103.
[16] J. H. Park, P. S. Krstic, *J. Phys: Condens. Matter* **2012**, in press.
[17] H. A. Pohl, *Dielectrophoresis: The Behavior of Neutral Matter in Nonuniform Electric Fields*, 2nd ed., Cambridge University Press, Cambridge, UK **1978**.
[18] T. B. Jones, *Electromagnetics of Particles*, Cambridge University Press, Cambridge, UK **1995**.
[19] P. R. C. Gascoyne, Y. Huang, R. Pethig, J. Vykoukal, F. F. Becker, *Meas. Sci. Technol.* **1992**, *3*, 439.
[20] N. G. Green, H. Morgan, *J. Phys. D: Appl. Phys.* **1997**, *30*, 2626.
[21] M. P. Hughes, H. Morgan, *J. Phys. D: Appl. Phys.* **1998**, *31*, 2205.
[22] H. Morgan, M. P. Hughes, N. G. Green, *Biophys. J.* **1999**, *77*, 516.
[23] R. Pethig, *Biomicrofluidics* **2010**, *4*, 022811.
[24] D. Branton, D. W. Deamer, A. Marziali, H. Bayley, S. A. Benner, T. Butler, M. Di Ventra, S. Garaj, A. Hibbs, X. Huang, S. B. Jovanovich, P. S. Krstić, S. Lindsay, X. S. Ling, C. H. Mastrangelo, A. Meller, J. S. Oliver, Y. V. Pershin, J. M. Ramsey, R. Riehn, G. V Soni, V. Tabard-Cossa, M. Wanunu, M. Wiggin, J. A. Schloss, *Nat. Biotechnol.* **2008**, *26*, 1146.
[25] P. K. Gupta, *Trends Biotechnol.* **2008**, *26*, 602.
[26] I. F. Sbalzarini, P. Koumoutsakos, *J. Struct. Biol.* **2005**, *151*, 182.

Received: August 24, 2011
Published online: January 23, 2012

NANO MICRO small

Supporting Information

for *Small*, DOI: 10.1002/smll.201101739

Tunable Aqueous Virtual Micropore

*Jae Hyun Park, Weihua Guan, Mark A. Reed, and Predrag S. Krstic´**

Supplementary Information for "Tunable Aqueous Virtual Pore"

Jae Hyun Park[1], Weihua Guan[2], Mark A. Reed[2,3] and Predrag S. Krstić[1]*

[1] Physics Division, Oak Ridge National Laboratory, Oak Ridge, TN 37831

[2] Department of Electrical Engineering, Yale University, New Haven, CT 06520

[3]Department of Applied Physics, Yale University, New Haven, CT 06520

*Corresponding Author: krsticp@ornl.gov

SI1. Stability of Aqueous Quadrupole Trap

The stability of AQT is different from the conventional Paul trap in vacuum or low-pressure gaseous medium, due to the presence of dielectrophoretic (DEP) force in addition to the electrophoretic (EP) force. Also, as mentioned in the text, the stability of AQ trap is determined by the mean motion (without random motion) of the particle under the assumption that the trap size is much larger than the random fluctuations. The equation of motion (EOM) in AQ trap including DEP as well as AC EP forces has the following form:

$$\frac{d^2x}{d\tau^2} = -b\frac{dx}{d\tau} + 2q\cos(2\tau)x + r_m\left[\mathrm{Re}(f_{CM}) + \mathrm{Re}(f_{CM})\cos(4\tau) - \mathrm{Im}(f_{CM})\sin(4\tau)\right]x \quad , \tag{SI1.1}$$

with introducing the dimensionless parameters of

$$\tau = \frac{\Omega}{2}t, b = \frac{2\xi}{M\Omega}, q = \frac{2QU}{MR_0^2\Omega^2}, r_m = \frac{4\alpha_m}{M\Omega^2}. \tag{SI1.2}$$

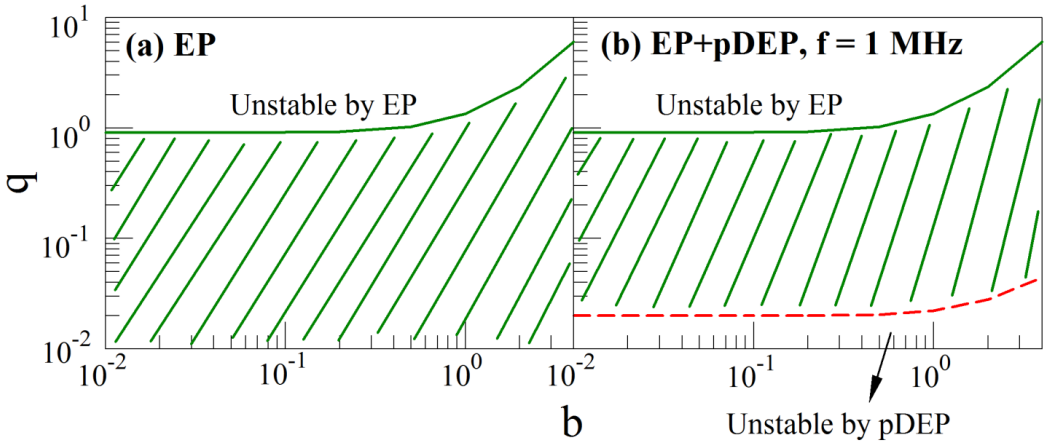

Figure S1. b-q Stability diagrams with a = 0.0 with/without pDEP: (a) EP; (b) EP+pDEP with f = 1.0 MHz. The lines are the stability borders. The green line is the stability border due to quadrupole electric field and the red dashed line is the border due to pDEP. The stable regions are the regions between the two borders (slanted lines).

By solving the EOM in Equation (SI1.1) and investigating the particle trajectory in long-time limit, we can determine the stability of trap. If the particle approaches the origin in long-time limit, the system is in the stable region for a given combination of b and q parameters. If the particle trajectory diverges from the origin, the system is unstable. The stability border is the (b,q)-relationship in which the trajectory keep oscillating without converging or diverging. The resultant (b,q)-stability diagram is shown in Figure S1. As shown in the Figure S1, for

small q's a new unstable region is generated whereas for the large q's the stability border is not influenced by the presence of DEP.

SI2. Details for the Equation of Motion, Equation (1)

The original two-dimensional equation of motion for the particle in AQT is given as:

$$\frac{d\,\mathbf{r}}{d\,\tau^2} = -b\frac{d\,\mathbf{r}}{d\,\tau} + 2q\cos 2\tau\left(x\hat{\mathbf{e}}_x - y\hat{\mathbf{e}}_y\right) + r_m\left[\mathrm{Re}\left(f_{CM}\right)\left(1+\cos 4\tau\right) - \mathrm{Im}\left(f_{CM}\right)\sin 4\tau\right]\left(x\hat{\mathbf{e}}_x - y\hat{\mathbf{e}}_y\right) \tag{SI2.1}$$

where $\mathbf{r} = x\hat{\mathbf{e}}_x + y\hat{\mathbf{e}}_y$ is the transformed coordinate vector. Here, x is the transformed coordinate in x-direction defined as x=(MΩ/2)X where X presents the physical coordinate and y is the transformed coordinate in y-direction defined as y=(MΩ/2)Y where Y presents the physical coordinate. τ = (Ω/2)t is the dimensionless time, ξ is the friction coefficient of a non-slip spherical particle in Stokes' drag, ξ=6πηa, where viscosity of medium, a is the particle radius. In the main text, we presents the x-component of Eq. (SI2.1). We also checked the results from y-component equation, however they did not change.

R is the white random force [S1] which vanishes in the mean:

$$\left\langle R(t)\right\rangle = 0, \tag{SI2.2}$$

and which is uncorrelated with the velocity $v(t)$ at any earlier time:

$$\left\langle v(t)R(t')\right\rangle = 0 \qquad t' > t. \tag{SI2.3}$$

where <> means the statistical average over an ensemble of particles. Finally, correlation time of R is infinitely short, namely the autocorrelation function of R(t) has the form,

$$\left\langle R(t)R(t')\right\rangle = G_R\delta(t-t'). \tag{SI2.4}$$

G_R is the constant spectral density in power spectrum of the random force. Kubo [S2] showed using fluctuation-dissipation theorem that G_R is related to the friction coefficient by

$$G_R = 2k_BT\xi. \tag{SI2.5}$$

The DEP force is not a function of charge. Since EOM in y-direction differs only in the sign of q-parameter and the stability diagram is symmetric with respect to q = 0, [S3] it is sufficient to solve the EOM in one direction (e.g. x).

SI3. Clausius-Mossoti Factor

Clausius-Mossoti factor is defined as $f_{CM} = \frac{\tilde{\varepsilon}_p - \tilde{\varepsilon}_m}{\tilde{\varepsilon}_p + 2\tilde{\varepsilon}_m}$ with $\tilde{\varepsilon} = \varepsilon_0 \varepsilon - j\frac{\sigma}{\Omega}$ where ε is relative dielectric constant and ε_0 is the vacuum permittivity (ε_0 = 8.85×10^{-12} F/m). The subscript p and m presents particle and medium, respectively. σ is the electric conductivity of material. j is imaginary unit $\left(j = \sqrt{-1}\right)$.

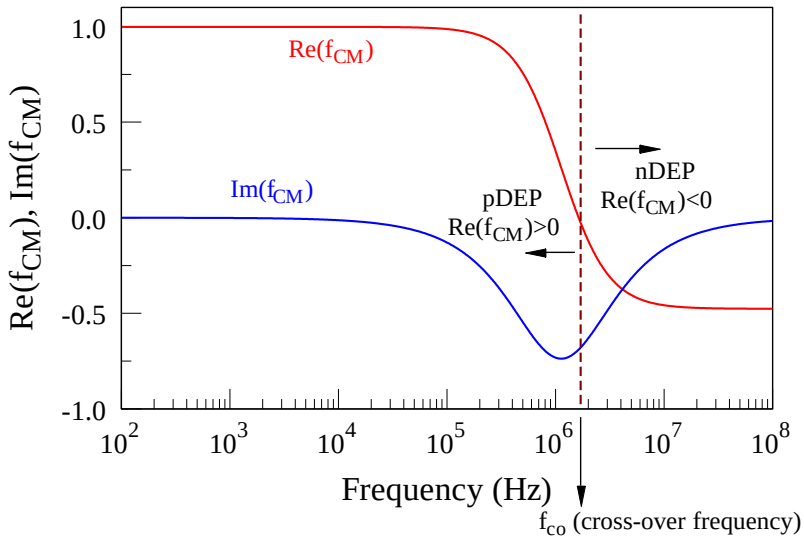

Figure S2. Typical Variation of Clausius-Mossoti (CM) factor, f_{CM}, with driving frequency. Re(f_{CM}) is the real and Im(f_{CM}) is the imaginary part of the f_{CM}, respectively. The cross-over frequency, f_{co}, indicates the frequency for which the sign of Re(f_{CM}) changes. For $f < f_{co}$, Re(f_{CM}) > 0 and the dielectrophoretic force acts toward the electrode (high electric field region), producing positive dielectrophoresis (pDEP) while for $f > f_{co}$, Re(f_{CM}) < 0 and the dielectrophoretic force acts toward the trap centre (low electric field region), producing negative dielectrophoresis (nDEP). For the polystyrene bead in aqueous medium, ε_p = 2.55 ε_m = 78.5 σ_p = 0.01 S/m σ_m = 5.5×10^{-6} S/m,[S4,S5] and the cross-over frequency is 1.63 MHz.

SI4. RMS Fluctuation v.s. q for EP-only Cases

The rms fluctuations without DEP can be calculated by solving Equation (1) with r_m = 0,

$$\frac{d^2x}{d\tau^2} + b\frac{dx}{d\tau} - 2q\cos(2\tau)x = \frac{2}{\Omega}R\left(\frac{2\tau}{\Omega}\right) \qquad \text{(SI4.1)}$$

The definitions of non-dimensional variables in the equation are explained in the main text and in SI3. Arnold *et al.* [S6] proposed an efficient numerical algorithm using Green function transformation and random phase approach, and we recently derived a closed form of rms fluctuations with Mathieu sine and cosine functions. We implemented both methods to

compute the rms fluctuations for various b and q parameters. Figure S3 shows the variation of rms fluctuations with q-parameters for three b-values of b = 1.0, 2.0, and 4.0. For all b-parameters, the rms fluctuations decrease with increase of q, reach the minima, and diverge.

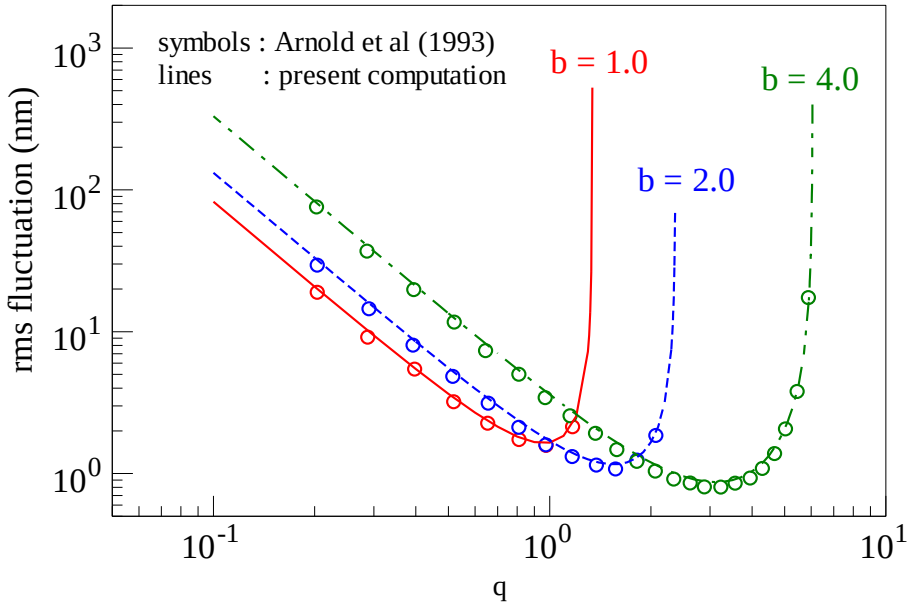

Figure S3. Variation of the rms fluctuations with q for three b-values of b=1.0, 2.0, and 4.0, The rms fluctuations are computed for the polystyrene bead whose radius is 490 nm and density of 1050 kg/m^3. The viscosity of medium is 0.89×10^{-3} Pa·s.

SI5. Means and Widths of the Radial Distributions of Particle

This section shows the means and widths of radial distributions of a particle in an aqueous virtual pore, due to the rms fluctuations. The mean value is defined as $\bar{r} = \left(\sum_{i=1}^{N} r_i\right) \Big/ N$ where N is the total number of events and r_i is the radial position of particle in each event. The width of radial distribution in Figure 2b and Figures 3(b-e), w_r, is defined as the standard deviation of the distribution, $w_r = \sqrt{\sigma_{rr}^2} = \sqrt{\left[\sum_{i=1}^{N}\left(r_i^2 - (\bar{r})^2\right)\right] \Big/ N}$.

Figures S4(a-b) show the profiles of mean (a) and the width (b) for Figure 2(b-c) in which the voltage varies with a fixed frequency. Figures 4(c-d) show the profiles of means (c) and the widths (d) for Figure 3(b-e) in which the frequency varies with a fixed voltage. The distributions of the calculated and measured means are similar, if the particle charge is properly chosen. For the fixed frequency cases (Figures S4a and b), the proper charge is

8×10^4 *e* while for the fixed voltage cases (Figures S4c and d), the proper charge is 4×10^4 *e*. The widths of the distributions are about a half of the means.

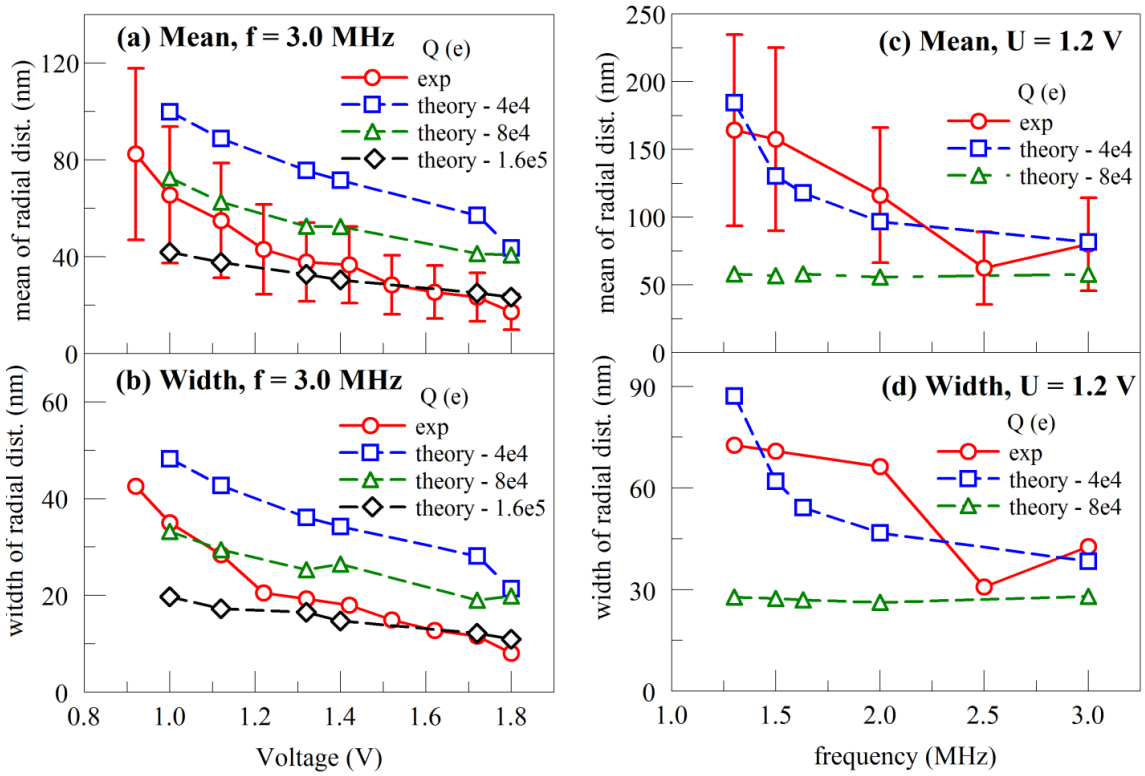

Figure S4. Measured and calculated means and widths of radial distributions when varying AC voltage and frequency: (a) means and (b) widths of radial distributions for a fixed frequency of f = 3.0 MHz. (c) mean and (d) width of radial distributions for a fixed voltage of U = 1.2 V. The error margins of the experimental data in (a) and (c) are about 40%.

SI6. Estimations of RMS Fluctuations with Variable Charges

In Figure 2a, we assumed that the charge is fixed regardless the variation of applied voltage. However, the comparison strongly suggests the possibility of variable charges depending on AC voltage. We selected four voltages of 1.0, 1.12, 1.32, and 1.72 V, for which the measured values exist. The estimation of the rms fluctuations with variable charges consists of three steps described in Figure S5. The first step is to construct the fitting relations between Q and rms fluctuations, modelled as $\sqrt{\bar{\sigma}_{xx}^{\infty}} = aQ^b$, for four different U's (Figure S5a). Interestingly, the exponents are always same as -0.62, while the pre-factor, *a*, is varied depending on the voltage. The second step is to build the fitting relation between U and Q, which can be successfully modelled with a linear relation $\frac{Q}{10^5 e} = cU + d$ (Figure S5b).

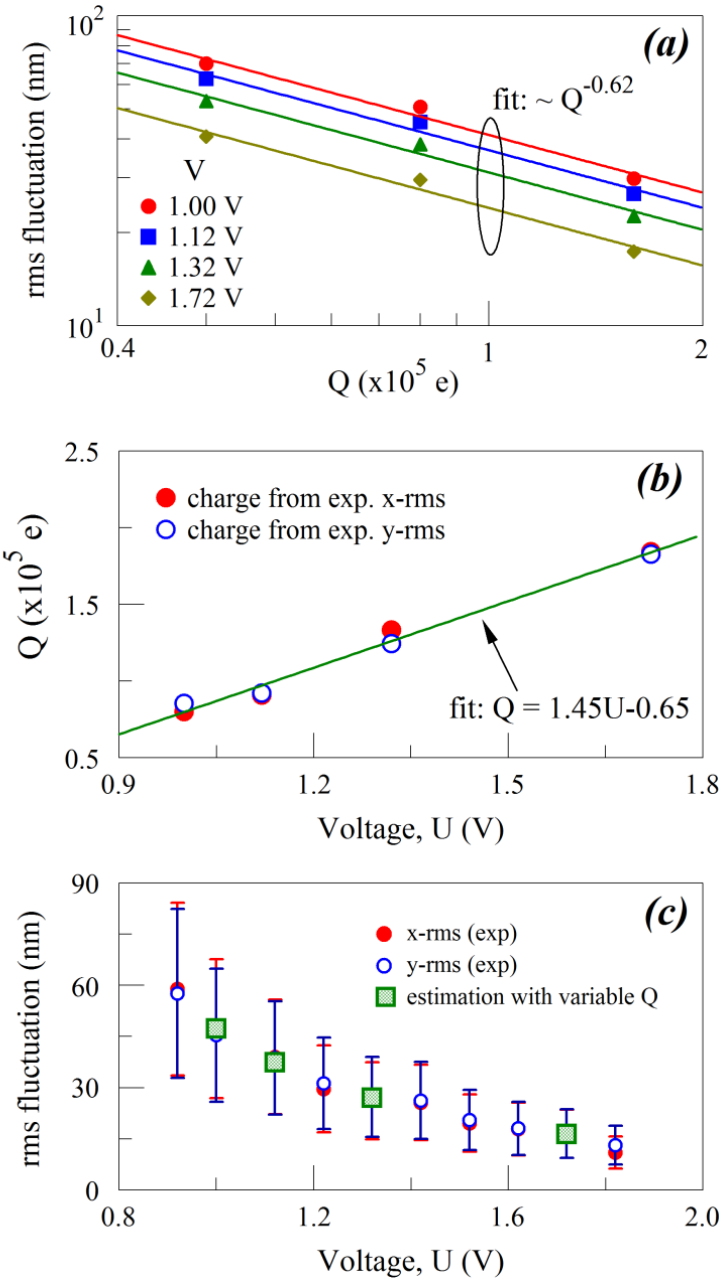

Figure S5. Estimation of rms fluctuations with variable charges: (a) STEP 1 – construction of fitting relations between Q and rms fluctuation for four different AC voltages of 1.0, 1.12, 1.32, and 1.72 V. The selected relation is $\sqrt{\bar{\sigma}_{xx}^{\infty}} = aQ^b$ for each voltage. The exponents of fitting relations are always obtained as -0.62 regardless of the voltage while the *a*-values are ranging from 41.25, 36.83, 31.25 to 24.00 nm with variation of voltages from 1.0, 1.12, 1.32, to 1.72 V, respectively; (b) STEP 2 – build a fitting relation of $\frac{Q}{10^5 e} = cU + d$ between U and Q. The c and d-values are 1.44 [V^{-1}] and -0.65, respectively. The charge is computed using the relation in (a) and the measured rms fluctuations; (c) STEP 3 – estimation of the rms fluctuations using the variable charge given by the relation in (b).

The charges are computed from the relation of $\sqrt{\bar{\sigma}_{xx}^{\infty}} = aQ^b$. The fitting parameters are 1.44 V^{-1} and -0.65 for c and d, respectively. Finally, using the two latest relations ($\sqrt{\bar{\sigma}_{xx}^{\infty}} = aQ^b$ and $\frac{Q}{10^5 e} = cU + d$) we can re-construct the voltage versus voltage plot (Figure S5c), to check the quality of the fits.

SI7. Trap Stiffness and Effects of Particle Size in AVP

As discussed by Guan *et al.*, [S7] the trap stiffness is derived as $k_{EP} = \frac{Q^2 U^2}{2M\Omega^2 r_0^4 \left[1+\left(\xi/M\Omega\right)^2\right]}$ for EP and $k_{DEP} = \left|\mathrm{Re}\left(f_{CM}\right)\right| \frac{2\pi\varepsilon_m\varepsilon_0 a^3 U^2}{r_0^4}$ for DEP, from the consideration of pondermotive components of each force. When the surface charge and mass densities are maintained constant with varying trap size proportionally to the particle size, ($Q = 4\pi a^2\sigma_s$, $r_0 = 8a$, $M = \rho_p \frac{4}{3}\pi a^3$, and $\xi = 6\pi\eta a$), $k_{EP} \propto a$ while $k_{DEP} \propto 1/a$.

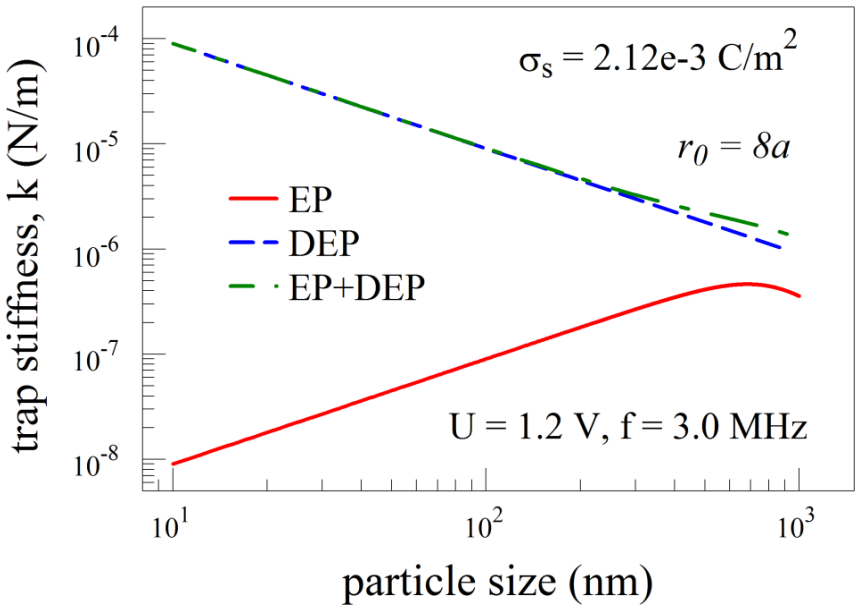

Figure S6. Variation of trap stiffness with the particle size. The particle is polystyrene with the density of 1050 kg/m^3. The trap size varies proportional to the particle size while the surface charge density is fixed as 2.12×10^{-3} C/m^2.

In Figure S7a, the surface charge density, σ_s, and the volume mass density, ρ_p, are maintained constant as in Figure S6. Note that in the experiment, the particle size is a = 490

nm and the trap size r_0 = 4 μm. This ratio is held fixed in all the calculations in Figure S7a. The EP rms fluctuations (r_m = 0) decrease with increase of the particle size whereas the DEP fluctuations (q = 0) increase with increase of the particle size. The total EP+DEP fluctuations ($q \neq 0$ and $r_m \neq 0$) increase with increase of particle size. However, the rms fluctuations increase with increase of the trap size, as shown in Figure S7b, while are reduced with increase of the particle charge (Figure S7c). In Figure 7d, we investigate the frequency effects for a small particle in a small trap ($2a$ = 10 nm and $2r_0$ = 81.63 nm) and a large particle in a large trap ($2a$ = 980 nm and $2r_0$ = 8 μm). For smaller case the AC voltage is reduced to 0.8 V to avoid the dielectric break-down in water.[S8] The rms fluctuations decrease with increase of frequency, and the decrement is significantly reduced for the smaller case.

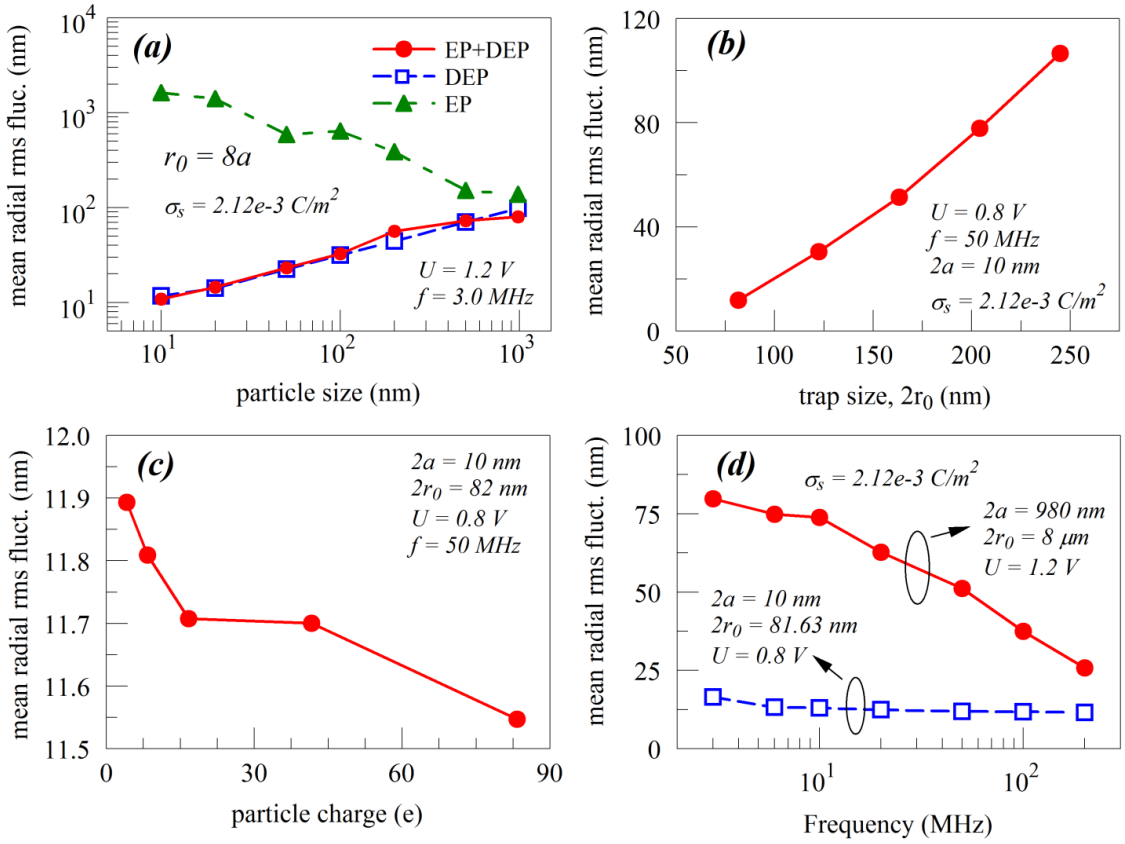

Figure S7: Variations of mean radial rms fluctuations with (a) particle size, (b) trap size, (c) particle charge, and (d) frequency.

References for Supplementary Information:

[S1] R. Kubo, *Rep. Prog. Phys*. **1996**, 29 255–284.

[S2] F. G. Major, V. N. Gheorghe, G. Werth, *Charged particle traps: physics and techniques of charged particle field confinement*, Springer, Berlin, **2005**.

[S3] W. T. Coffey, Yu. P. Kalmykov, J. T. Waldron, *The Langevin equation: with applications to stochastic problems in physics, chemistry and electrical engineering*, 2nd ed. World Scientific Publishing Co., Singapore, **2004**.

[S4] N. G. Green and H. Morgan, *J. Phys. Chem. B* **1999**, 103, 41-50.

[S5] S. Park and A. Beskok, *Anal. Chem.* **2008,** 80, 2832-2841.

[S6] S. Arnold, L. M. Folan, A. Korn, *J. Appl. Phys.*, **1993**, 74, 4291-4297.

[S7] W. Guan, J. H. Park, P. S. Krstić, M. A. Reed, *Nanotechnology*, **2011**, 22, 245103.

[S8] W. A. Stygar, T. C. Wagoner, H. C. Ives, Z. R. Wallace, V. Anaya, J. P. Corley, M. E. Cuneo, H. C. Harjes, J. A. Lott, G. R. Mowrer, E. A. Puetz, T. A. Thompson, S. E. Tripp, J. P. VanDevender, J. R. Woodworth, Phys. Rev. ST Accel. Beams **2006**, 9, 070401.